Annealing effect on structural, microstructural and electrical properties of ZnS nanoparticles synthesized in aqueous medium

Afef Yacoubi, Tahar Ben Chaabane*

Unité de Recherche Synthèse et Structure de Nanomatériaux UR 11 ES 30. Faculté des Sciences de Bizerte, 7021 Jarzouna, Bizerte. Université de Carthage, Tunisie.

(Received: 20 September 2015, accepted: 04 April 2016)

Abstract: Nanocrystalline zinc sulfide (ZnS) was synthesized by simple chemical precipitation in aqueous medium at 80°C using zinc nitrate and thioacetamide (TAA) as reactants. The prepared products were annealed in air at different temperatures in the range of 500–650°C. The as-prepared and annealed samples were characterized by different techniques. The structure and morphology of the products were characterized by X-ray diffraction (XRD), transmission electron microscopy (TEM), Fourier transform infra-red (FT-IR) and Energy-Dispersive X-ray (EDX) spectroscopies. From the XRD and FT-IR analysis, the crystal structure is found to convert from cubic ZnS phase to the hexagonal ZnO phase with the increasing annealing temperatures. The electrical properties of ZnO nanopowder were investigated using impedance spectroscopy. The electrical conductivity increases with increasing temperature with a typical Arrhenius-type behaviour. The Arrhenius plot presented two linear portions indicating tow dominant mechanisms affecting the electrical conductivity of ZnO.

Keywords: Zinc sulphide/ Zinc oxide/ Annealing effect/ Nanoparticles/ Nanotechnology/ Impedance spectroscopy/ Electrical conductivity/ Activation energy

INTRODUCTION

Many research activities have been devoted to the synthesis and characterization of semiconductor nanoparticles. This interest is due to their unique physical and chemical properties that cannot be observed in bulk semi-conductor materials [1-5]. Such singular characteristics are originated from their large surface-to-volume ratio and confinement phenomena such as atomic-like electronic structure with discrete energy levels.

Among the various II-VI semiconductors, ZnS is an important material with a direct wide band gap of 3.66 eV [6,7]. It is chemically more stable and technologically better than the other zinc chalcogenides. Zinc sulfide nanomaterial exhibits novel properties which are at the origin of diverse promising applications such as ultraviolet light sensors [8], efficient UV light emitting diodes [9], optoelectronic devices [10] and electroluminescent applications [11].

On the other hand, zinc oxide (ZnO) is also a kind of important semiconductor, having a large band gap and possesses unique optical and electronic properties. It is regarded as the promising material applied in nanotechnology and photocatalysis.

Various synthesis methods have been used to obtain ZnS nanocrystals with reproducible sizes and morphologies. ZnS nanoparticles have been produced using polyol process [12, 13], sulfate salts calcination method [14], solvothermal route [15-17], ball-milling [18] etc.

It is worth to note that previous studies have focused on the electrical properties of doped [19-20] or undoped [21-22] ZnO material. The effect of the particles shape and size on the electrical conductivity of ZnO was also investigated. H. Wang et al. [23] have prepared ZnO samples with different morphologies (rods, fusiform-like, flower -like,…). The authors have found different electrical conductivities depending on the sample morphology, the highest conductivity was determined for the fusiform-shaped ZnO sample. M. Orvatinia and R. Imani have studied the

* Corresponding author, e-mail address : taharbch@yahoo.com

electrical conductivity of ZnO nanowires films [24]. The nanowires have different lengths and diameters depending on the synthesis temperature varying in the range: 750°C-950°C. The ZnO nanowires prepared at lower temperature have a higher length and thinner diameter. The authors have recorded the conductivity variation of the samples as a function of inverse temperature according to Arrhenius model. They have found two activation energies E1 and E2 corresponding to two dominant mechanisms and the values of E1 and E2 increase when the synthesis temperature increases.

In this paper, nanometer-scale ZnS particles were synthesized via simple chemical precipitation method in aqueous medium [25-26]. The starting compounds were zinc nitrate as Zn source and thioacetamide as sulfide source material [27]. The probable reaction process for the formation of ZnS particles can be proposed as follows [28]:

$$CH_3CSNH_2 + H_2O \rightarrow CH_3CONH_2 + H_2S$$
$$H_2S \rightarrow 2H^+ + 2S^{2-}$$
$$Zn^{2+} + S^{2-} \rightarrow ZnS$$

Annealing the as-prepared ZnS nanoparticles leads to ZnO product. The annealing effects on structural and microstructural properties of zinc sulfide nanoparticles were studied. Note that the electrical properties of ZnO nanocrystals can be affected by various factors: the synthesis process, the size and the shape of the particles, the existence of native point defects and impurities, hence we are interested to study the electrical properties which are investigated and discussed for the ZnO nanoparticles obtained with quasi-spherical shape.

EXPERIMENTAL SECTION

1. Synthesis of ZnS nanoparticles

Zinc nitrate hexahydrate ($Zn(NO_3)_2.6H_2O$, 98 %) and thioacetamide (CH_3CSNH_2, 99 %) were used as received without additional purification. All solutions were prepared using ultra-pure water.

ZnS nanoparticles were synthesized in aqueous medium. In typical procedure, 3.710 g of zinc nitrate hexahydrate was dissolved in ultra-pure water (0.5M). A separated solution containing 1.120 g of thioacetamide dissolved in water (0.5M) was also prepared and added drop wise to zinc nitrate solution under magnetic stirring. The mixture was then placed in a flask and heated to 80°C for 3h under continuous mechanical agitation. After cooling to room temperature, the precipitate was centrifuged, washed several times with ethanol and acetone, and then dried in air at 60°C.

The synthesized products were placed into crucible and annealed in air for three hours at different temperatures in the range of 500-650 °C.

2. Characterization

The X-ray powder diffraction (XRD) patterns were recorded on a Bruker D8 Advance apparatus with Cu(K_α) radiation (λ = 1.5406 Å). The average crystallite sizes were calculated from the width of the XRD peaks using the Scherrer formula [29].

Transmission electron microscopy (TEM) images were taken by placing a drop of the particles in water onto a carbon film-supported copper grid, the size and the shape of the particles were determined using a Tecnai Transmission Electron Microscopy operating at 200 kV equipped with an energy dispersive Spectrometer (EDX).

Fourier transform infrared (FT-IR) spectra were recorded on a Thermo Scientific Nicolet IR 200 spectrophotometer in the range of 400-4000 cm^{-1}.

For electrical measurements, the powders were pressed into pellets and sintered in air at 550°C for 2h. Electrodes have been prepared by painting silver on both sides of the sintered pellet to ensure good electrical contact.

Impedance measurements were recorded from room temperature to 240°C with stabilization time of 10 min between consecutive measurements. The frequencies were ranging between 10 Hz and 13MHz and the measurements were performed using a Hewlett Packard HP 4192A impedance analyzer.

RESULTS AND DISCUSSION

1. Structural and microstructural characterizations

XRD patterns of the recuperated powder as well as those of annealed samples are recorded in the scan range 2θ = 10-60° (Figure 1). All the diffraction peak positions of the as-prepared powder (Fig.1a) are in good accordance with the data reported in JCPDS No. 05-0566 [30] corresponding to ZnS cubic phase. The peak broadening in the XRD patterns clearly indicated the nature of the small nanocrystals. Crystallite size of the nanoparticles was estimated following the well-known Sherrer equation:

$L = 0.9\lambda/(\beta\cos\theta)$ where L represents crystallite size (Å), λ is the wavelength of Cu(Kα) radiation

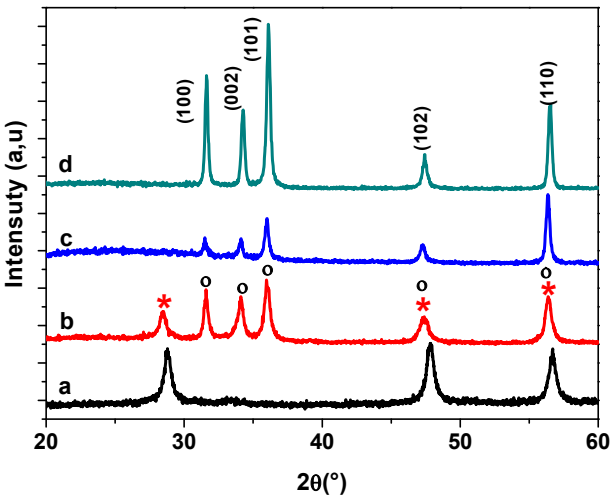

Figure 1: X-ray diffraction (XRD) of pure as-prepared ZnS (a), ZnS annealed at 500°C (b), 550°C (c) and 650 °C (d) (* and ^{0} for ZnS and ZnO diffraction peaks respectively).

Table I: Diffraction angle positions, FWHM and (h k l) planes of the main diffraction peaks of ZnO phase obtained at different annealing temperature. Their corresponding calculated crystallite sizes are also given.

T (°C)	2 θ	(hkl)	FWHM	Size (nm)	Average size (nm)
550	31.48	(100)	0.307	39.9	35
	34.07	(002)	0.361	31.7	
	35.95	(101)	0.341	34.7	
650	31.59	(100)	0.219	67.1	58
	34.23	(002)	0.243	57.3	
	36.17	(101)	0.280	48.2	

(Å) and β is the corrected full width at half maximum (FWHM) of the diffraction peak. The calculated crystallite size of the as-prepared sample (Figure1a) was determined to be 17.5 nm.

The XRD pattern of the ZnS sample annealed at 500°C (Figure1b) revealed that the ZnO phase has set in with the presence of cubic phase of ZnS resulting in the formation of a zinc blende-wurtzite ZnO mixed phases. Increasing the annealing temperature to 550°C leads to completely disappearance of ZnS cubic phase because the corresponding XRD pattern (Figure1c) shows only the characteristic diffraction peaks of the hexagonal zinc oxide. According to bibliography, the conversion of the annealed ZnS nanoparticles to ZnO hexagonal phase can occur in air in the temperature range of 550°C-600 °C [31, 32]. The XRD diagram of the ZnS sample calcined at 650° C is shown in Figure1d. It exhibited well crystallized powder with diffraction peaks related to the lattice planes of (100), (002), (101), (102) and (110) which are consistent with the ZnO wurtzite phase as reported in ICDD card N° 70-8070 [33]. It is worth to note that on further increasing the annealing temperature up to 650°C, the diffraction peaks are found to narrow down and their intensity increases as compared to those of the sample annealed to 550°C. The corresponding calculated crystallite sizes are increased to reach an average value of 58 nm (Table I).

In order to elucidate the morphology of the

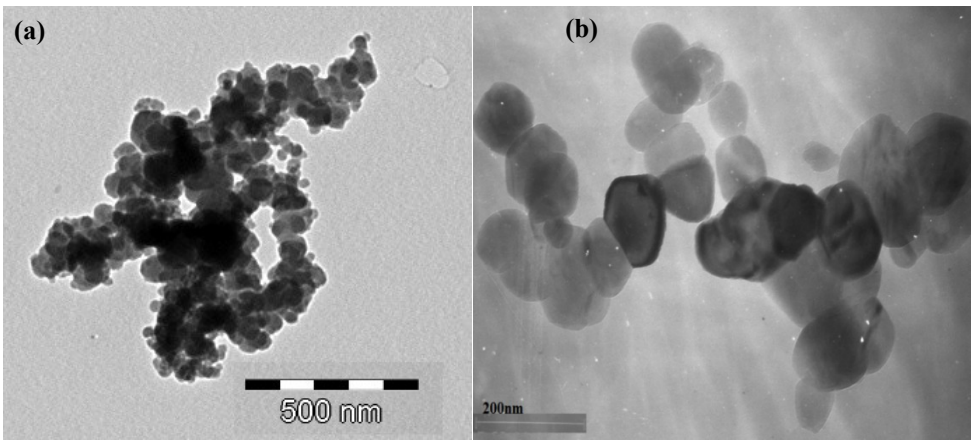

Figure 2: TEM images of ZnS nanocrystals for as-prepared sample (a) and annealed sample at 650°C (b).

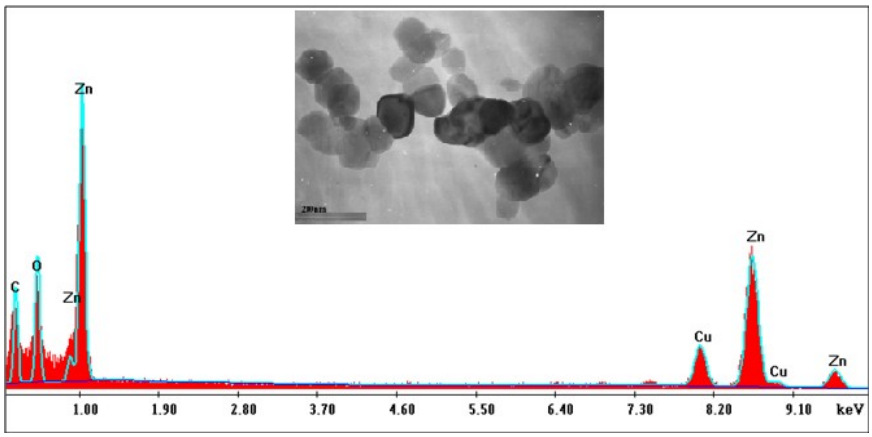

Figure 3: EDX spectrum of the ZnS annealed at 650°C.

obtained particles, transmission electron microscopy (TEM) investigation was performed. Typical TEM images of as-prepared sample and annealed one at 650°C samples are given in figure 2a and 2b respectively. TEM image of the starting powder (Figure2a) shows spherical particle strongly aggregated with diameters ranging in 80-100 nm and are constituted by nanometer-sized crystals of about 20 nm. The TEM image of the calcined sample at 650°C (Figure 2b) shows less agglomerated quasi-spherical particles with size ranging in 60-80 nm. The observed particles diameters are in accordance with the calculated crystallite sizes obtained from the XRD patterns (Table I).

Energy Dispersive X-ray Spectrometry (EDX) was used for the elemental analysis of the annealed ZnS nanoparticles at 650°C. The EDX spectrum of the sample is shown in figure 3. The observed signals of carbon and copper must be omitted because they originate from the carbon film and the copper gird used for the sample preparation. The intense peaks belong to Zn and O elements and there are no other impurity elements in the sample. Then EDX analysis indicates good purity of the product in one hand and proves the complete oxidation of ZnS into ZnO in the other hand.

2. FT-IR spectroscopy analysis

The infra-red spectra of the as-prepared sample and the annealed ZnS ones are given in Figure 4. For the starting material spectrum (Figure 4a), the broad band at 3414 cm^{-1} and the less intense one at 1640 cm^{-1} are correlated to the water and hydroxyl vibrations respectively. The bands located at 1316 and 817 cm^{-1} are due to NO_3^- group [34]. The peak observed around 1460 cm^{-1} can be originated from C-H stretching of thioacetamide precursor. The bands located at 1046 and 640 cm^{-1} are ascribed to the formation of Zinc sulfide [35, 36]. For the ZnS annealed at 500°C (Figure 4b), the vibration bands assigned to nitrate groups, C-H bond and those originated from water disappear whereas a new strong vibration band located at 429 cm^{-1} with a shoulder at 483 cm^{-1} appears. These latter wave numbers are characteristic of ZnO vibration [37, 38].

The infra-red spectra of the annealed ZnS at 650°C particularly reveal that the specific vibration band of Zn-O becomes dominant indicating the complete oxidation of the zinc sulfide particles.

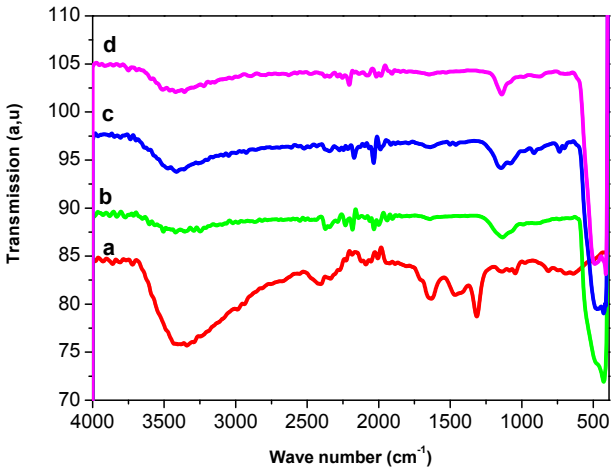

Figure 4: FTIR spectra of ZnS nanoparticles: as-prepared (a), annealed at 500 ◦C (b), annealed at 550 ◦C (c) and annealed at 650°C (d).

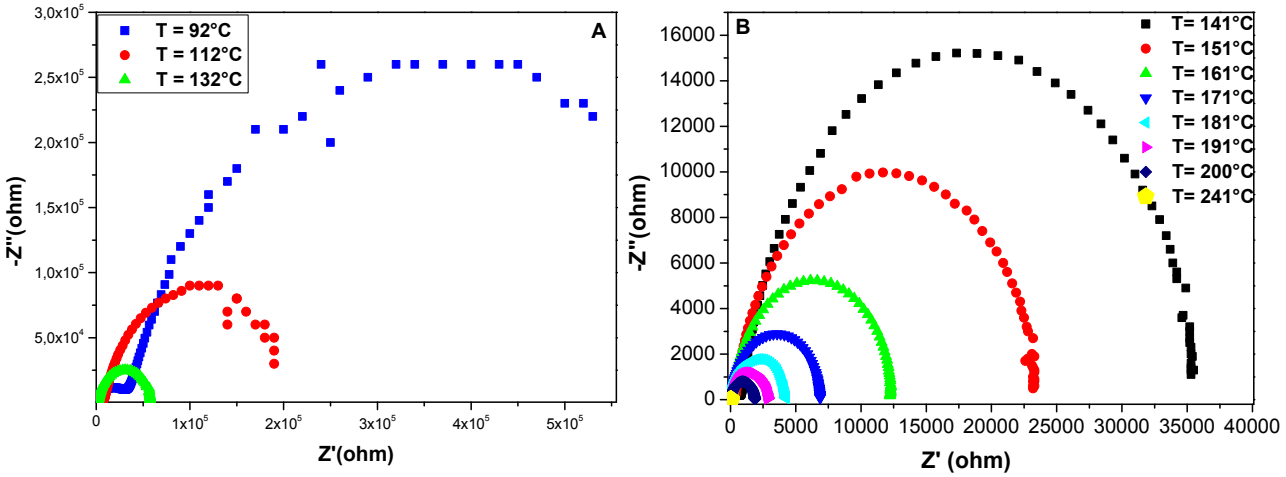

Figure 5: Nyquist plots for ZnO nanoparticles (A: temperature range: 92-132 °C; B: temperature range : 141-241 °C)

3. Electrical properties

Complex plots of imaginary part of impedance -Z'' versus the real part Z' of ZnS annealed at 650° C are displayed for different temperatures in Figure 5 in which semicircles are obtained. The sample resistances R as function of the temperature have been obtained from the values of the intercept of the extrapolated semicircles with the real axis. The corresponding conductivities σ were calculated in accordance with the relation: $\sigma = L/RS$ where S and L are area and thickness of sample pellet, respectively. Each impedance spectrum is characterized by the appearance of a single semicircular arc whose radius of curvature decreases as temperature increases. The resistance values decrease and then the conductivities increase with the temperature indicating semi-conducting behaviour of the sample. It is well known that undoped ZnO presents n-type conductivity due to the formation of native donor-type defects related to oxygen vacancy (VO) and zinc interstitial (Zn_i) [39]. Increasing the number of such defects multiplies the number of electrons as charge carrier and then enhances the conductivity of ZnO material.

The observed one-arc spectrum in figure 5 means that the sample conduction in the grain and the grain boundary occurs in the same process leading to the same semicircle. Nevertheless, Jose et al [40] and Nan et al. [41] have studied the impedance spectra for nanostructured Zinc oxide, the ZnO specimens were prepared only by pressing without sintering and the authors obtained impedance spectra exhibiting two arcs. The low frequency arc is due to the grain boundary effect and the high frequency one is attributed to the grain effect. Z. Zhou et al. have compared the impedance spectra of pure ZnO specimens with and without sintering; the authors have obtained impedance spectra with single arc for the former and tow arcs for the latter [42].

Typical Arrhenius-type behaviour with linear dependence of thermal conductivity logarithm log (σ. T) on inverse of temperature $10^3/T$ (K^{-1}) is shown in Figure 6. The linear relationship was in accordance with the following expression: $\sigma.T = \sigma_0 \exp(-E/kT)$, where σ_0 is the pre-exponential factor, E the activation energy, T the absolute temperature and k the Boltzmann constant. Therefore, the temperature dependence of the conductivity clearly indicates that the electrical conduction in ZnO sample is a thermally activated process. Tow linear portions were obtained in figure 6, they are indicative of different activation energy E1 = 0.90 eV and E2 = 0.16 eV corresponding to tow temperature regions. E1 and E2 are determined in the high and low temperature range respectively, they present tow values remarkably distinct. The determined transition temperature was found to be 114°C (387 K) which is in agreement with M. Orvatinia and R. Imani study concerning the electrical conductivity of different ZnO films [24].

The activation energy represents the location of trap levels below the conduction band. The distinct values of E1 and E2 indicate the presence of two donor levels. These levels are the shallow and deep donor levels in the band gap of the ZnO semi-

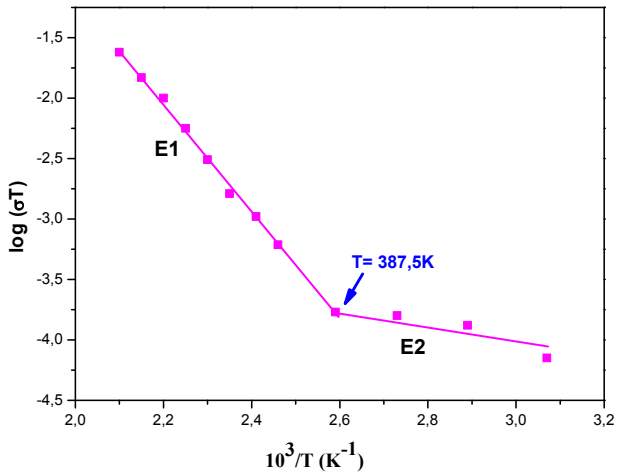

Figure 6: Arrhenius plot of log (σ T) versus 1000/T of ZnO nanoparticles.

conductor. The lower value of 0.16 eV corresponds to the shallow donor level, while the higher value of 0.90 eV corresponds to the deep donor level.

CONCLUSION

ZnS nanoparticles were synthesized by simple precipitation in aqueous phase from zinc nitrate and thioacetamide. The prepared powder exhibits cubic blende phase with high degrees of purity and crystallinity. The zinc sulfide product was annealed at 500, 550 and 650°C and the crystal structure started to convert from cubic ZnS phase to the wurtzite ZnO phase from the temperature of 500° C. The annealed ZnS sample at 650° C exhibited well crystallized ZnO phase with high purity. The electrical conductivity of the latter product increases with the increase of the temperature in accordance with the semi-conducting behaviour of the material. ZnO exhibited two distinct activation energies corresponding to tow conduction mechanisms which occur in different temperature regions.

REFERENCES

[1] W. Xie, C. Chen , *Physica B: Condensed Matter.*, **1999**, 266, p.373..
[2] N. Tokio, F. Keisuke, K. Akio, *Journal IEEE Transactions on Electron Devices.*, **1999**, 46, p.11.
[3] C. Falcony, M. Garcia, A. Ortiz, *J. C. Alonso'Journal of Applied Physics.*, **1992**, 72, p.1525.
[4] W. Tang, D.C. Cameron, *Thin Solid Films.*, **1996**, 280, p.221.
[5] M.A. Ledger, *Applied .Optics.*, **1979,** 18, p. 2979.
[6] H.Y. Lu, S.-Y. Chu, S.-S. Tan, *Journal of Crystal Growth*, **2004**, 269, p.385.
[7] K.R. Murali, A.C. Dhanemozh, R. John, *J. Alloy. Compd.*, **2008**, 464, p.383.
[8] X. Fang, Y. Bando, M. Liao, T. Zhai, U.K. Gautam, L. Li, Y. Koide, D. Golbe, *adv. Funct. Mater.*, **2010**, 20, p.500.
[9] C. Rui, L. Dehui, L. Bo, P. Zeping, G.G. Gagik, X. Qihua, S. Handong, *Nano Letters.*, **2010**, 10, p.4956.
[10] M. Kastner 'Artificial atoms' *Physics Today.*, 46, p.24.
[11] V. L. Colvin, M. C. Schlamp, A. P. Alivisatos, *Nature.*, **1994**, 370, p.354.
[12] C. Feldmann, C. Metzmacher, *J. Mater .Chem.*, **2001**, 11, p.2603.
[13] Y. W. Zhao, Y. Zhang, H. Zhu, G. C. Hadjipanayis and J. Q. Xiao, *J .Amer .Chem .Society.*, **200**4, 126, p.6874.
[14] Y. He, J. Wang, *Mater Lett.*, **2008**, 62, p.1379.
[15] L. Yadong, D.Yi, Z.Yue, Q. Yitai, *J. Phys. Chem. Solids.*, **1999**, 60, p.13.
[16] J. Changlong, Z. Wangqun, Z. Guifu Y. Weicao, Q. Yitai, *Mater. Chem. Phys.*, **2007**,103, p.24.
[17] M. Jayalakshmi, M.M. Rao, *J.Pow. sour.*, **2006**, 157, p. 624.
[18] P. Baláž, E. Boldižárová, J. Briančin , *Mater Lett.*, **2003**, 57, p. 1585.
[19] R. Saravanan, T. Prakash, V.K. Gupta, A. Stephen, *J. Mol. Liq.*, **2014**, 193, p.160.
[20] A. Tabib, N. Sdiri, H. Elhouichet, M. Férid, *J. Alloy. Compd.*, **2015**, 622, p.687.
[21] Ce-W. Nan, A. Tschöpe, S. Holten, H. Kliem, R. Birringer, *J. Appl. Phys.*, **1999**, 85, p.1.
[22] M. Caglar, S. Ilican, Y. Caglar, F. Yakuphanoglu, *Appl. Surf. Sci.*, **2009**, 255, p.4491.
[23] H. Wang, C. Li, H. Zhao, Ru Li, J. Liu, *Powder .Technol.*, **2013**, 239, p.266.
[24] M. Orvatinia, R. Imani, *Int. J. Nanosci.*, **2012**, 11, p.1250032
[25] H. Labiadh, T. Ben.Chaabanen, D. Pitkowski, S. Mackowski, J. Lalevée, J. Ghanbaja, F. Aldeek, R. Schneider, *Mater.Chem. Phys.*, **2013**, 140, p. 674.
[26] H. Labiadh, T.Ben.Chaabane, L.Balan, N. Becheik, S.Corbel, G.Medjahdi, R.Schneider, *Appl.Catal.B.*, **2014**, 144, p.29.
[27] X. Yan, E. Michael, S. Komarneni, J.R. Brownson Zi-F. Yan, *Ceramics. International.*, **2013**, 39, p.4757.
[28] F. Gu, C. Zhong Li, S.F. Wang, M.K. Lu, *Langmuir.*, **2006**, 22, p.1329
[29] W. M. Hua, F. Zhou, B. Zhang, C. Yao, *J. Alloy .Comp.*, **2013**, .581, p.308.
[30] S.K. Panda, A Datta, S Chaudhuri, *Chem. Phys. Lett.*, **2007**, 44, p.235.
[31] R. Amaranatha, G. Murali, B. Poornaprakash, R.P. Vijayalakshmi, B.K.Reddy, *Solid.State.Commu.*, **2012**, 152, p.596.

[32] H. Z. Zeng, K.Q. Qiu, Y.Y. Du, W.Z. Li, Chin. *Chem .Lett.,* **2007**, 18, p.483.
[33] H. Kaftelen, K. Ocakoglu, R. Thomann, S. Tu, S. Weber, E. Erdem, *Phys. Rev. B.*, **2012**, 86, p.014113.
[34] W. Rizwan, S.G. Ansari, S.H-Kee, Y. S. Kim, E.-K. Suh, H.-S. Shin, *Solid .State.Sci.,* **2009**, 11, p.439.
[35] T.Y. Yesu, R. Anitha, B. Kavitha, *Appl. Sci. Res.,* **2012**, 1, p.282.
[36] S.R. Annie, S.P.Joseph, C. Muthamizhchelvan, *J, Chem.Tech.,* **2015**, 7, p.571.
[37] N. Rajeswari, A. Yogamolar, *J. Alloy. Compd.,* **2011**, 509, p.8493.
[38]G. Xiong, U.Pal, J. Serrano, *J. Appl. Phys.*, **2007**, 101, p.024317.
[39] L. Yow-Jon, T. Chia-Lung, L. Yang-Ming, L. Chia -Jyi, *J. Appl. Phys.,* **2006**, 99, p.93501.
[40] J. Jose, K. Abdul K, *Mat. Sci. Eng:A.,* **2001**, 304-306, p.810.
[41] C. Nan, A.Tschöpe, S. Holten, H. Kliem, R.Birringer, *J. Appl. Phys.,* **1999**, 85, p.7735.
[42] Z. Zhen, k.Kato, T. Komaki, M. Yoshino, H. Yukawa, *J .Eur .Ceram .Soc.,* **200**4, 24, p.139.